

Structures of Platinum Clusters: Planar or Spherical?[†]

Li Xiao and Lichang Wang*

Department of Chemistry and Biochemistry, Southern Illinois University, Carbondale, Illinois 62901

Received: April 5, 2004; In Final Form: May 20, 2004

Platinum clusters of up to 55 atoms were studied using density functional theory with a plane wave basis set. The results show that planar platinum clusters of up to nine atoms are as stable as their three-dimensional isomers and the six-atom planar cluster is, surprisingly, more stable than its three-dimensional isomers. Among the three-dimensional platinum clusters investigated in this work, the layered clusters are found to be as stable as their spherical close-packed isomers. The high stability of planar and layered clusters suggests that it is easy to grow a platinum monolayer or multilayer. The existence of many energetically possible isomers shows a fluxional structural characteristic of platinum clusters. The effect of the spin–orbit coupling was investigated, and the results show that the relative stability of the Pt clusters is not affected although the binding energy of the cluster increases if the spin–orbit coupling is included in the calculation. Most of the platinum clusters studied here show good conductivity and ferromagnetism, which make them potentially useful as high-density magnetic data storage materials. A quantitative correlation is provided between various properties of platinum clusters and the structure and size.

1. Introduction

Small clusters have attracted great attention in recent years due to their high ratio of surface area to volume and the finite spacing of energy levels with respect to their bulk counterparts.¹ In particular, transition metal clusters have been of special interest both theoretically and experimentally because of their potential as catalysts and high-density magnetic data storage materials.^{2,3} Platinum is one of the ingredients in the catalyst used in automotive catalytic converters to reduce toxic pollutants, such as CO, NO_x, and hydrocarbons, and is also an important material for the heterogeneous catalysis of hydrogenation. It has long been recognized that size and microstructures of metal particles play important roles in their catalytic performance, though little is known about how the catalytic behaviors of these nanoparticles depend quantitatively on their size and structures.³ In addition, tremendous effort has been made toward increasing magnetic data storage capacity. The evidence of ferromagnetism of metal clusters makes research on these nanoparticles particularly attractive due to their potential as high-density magnetic data storage materials.^{2,4,5} Therefore, studies on the mechanical and electromagnetic properties of the platinum clusters as well as their relationships to size and shape will advance our understanding of these nanoparticles as well as their applications in the chemical and materials industry.

Small Pt clusters ($n = 2–12$) have been investigated in detail by several groups using different methods.^{6–29} Theoretical studies of Pt dimer show that the bond lengths of low-lying electronic states are in the range of 2.4–2.6 Å, which are shorter than the bulk Pt–Pt bond length of 2.77 Å, and the spin–orbital effects are significant as demonstrated by complete active space MCSCF (CASSCF) followed by first-order configuration interaction calculations.⁶ The MP2 calculations show a hybridization among 6s, 6p, and 5d atomic orbitals in the formation of

the Pt–Pt bond.⁷ On the other hand, studies on the electronic states of platinum trimer using an ab initio generalized valence bond method⁸ show that the Pt–Pt bonding is dominated by delocalized s–s interactions and the overlap of a 6s–6s bond is maximized by the s–d hybridization with a negligible s–p hybridization.

Despite many studies of Pt clusters, there are controversies with regard to the ground-state structures. A density functional theory study of Pt clusters with four to six atoms based on the non-self-consistent Harris functional version of the local density approximation (LDA) indicates that the planar structure is more stable than the three-dimensional structure.⁹ In contrast, the results obtained from the B3PW91 calculations show that the most stable structure is tetrahedral among four-atom Pt clusters and square-based pyramidal among five-atom Pt clusters.¹⁰ Obviously, those structures need to be reexamined.

The 13-atom and 55-atom Pt clusters have also drawn much attention because they can form closed-shell icosahedral and cubooctahedral structures.^{31–38} Despite many studies on the 13-atom Pt clusters, what is the most stable structure of the 13-atom clusters is still an issue in debate. For instance, other isomers with lower energies than the icosahedral and cubooctahedral structures are found using the many-body embedded atom method.³² On the other hand, different embedded atom method calculations show that the icosahedron is the most stable structure.^{14,33}

Moreover, for systems involving Pt atoms, relativistic effects are expected to be important.^{12,18a,30} However, spin–orbit coupling was not taken into consideration in most previous calculations. In this paper, we present our investigation of 70 Pt clusters that consist of 2–55 atoms using density functional theory (DFT) calculations with a plane wave basis set. We will focus on investigating the following three issues. First, is the planar or three-dimensional isomer more stable? Second, is the icosahedral or cubooctahedral structure or the other layered structure more stable? Third, how does the spin–orbit coupling affect the binding energy of the Pt cluster? Furthermore, the

[†] Part of the “Gert D. Billing Memorial Issue”.

* To whom correspondence should be addressed. Phone: (618) 453-6476. Fax: (618) 453-6408. E-mail: lwang@chem.siu.edu.

TABLE 1: Binding Energies (E_B), Bonding Energies (E_{bond}), HOMO–LUMO Band Gaps (E_G), Magnetic Moments (μ), and Bond Distances of Linear Pt Chains

Notation	L ₂	L ₃	L ₄	L ₅	L ₆
Structure					
E_B (eV/atom)	1.76	2.18	2.32	2.53	2.52
E_{bond} (eV/bond)	3.52	3.27	3.09	3.16	3.02
E_G (eV)	0.81	1.71	0.00	0.53	0.19
μ (μ_B /atom)	1.00	1.33	0.50	0.00	0.33
Notation	L ₇	L ₈	L ₉	L _{∞}	
Structure					
E_B (eV/atom)	2.57	2.61	2.63	2.85	
E_{bond} (eV/bond)	3.00	2.98	2.96	2.85	
E_G (eV)	0.17	0.16	0.04	0.00	
μ (μ_B /atom)	0.29	0.38	0.22	0.00	

large number of Pt clusters studied here allows us to correlate the electromagnetic properties of Pt clusters with the cluster size and structure. This work also provides us the data to be used for constructing a potential energy surface that is necessary in our future dynamics studies on the catalytic behaviors of Pt nanoparticles and allows us to correlate the catalytic activities of these nanoparticles with their magnetic properties.

2. Computational Details

Among 70 Pt clusters investigated in this work, many isomers have been studied and compared for the stability, the energy gap between the highest occupied molecular orbital and the lowest unoccupied molecular orbital (HOMO–LUMO), and the magnetic moment. In addition to the three-dimensional structures, the one-dimensional and two-dimensional structures were also studied. Initial structures were chosen according to our experience on studies of other transition metal clusters^{39–41} and were relaxed without imposing any symmetry constraints.

The simulation techniques used here are similar to those in our previous studies.^{39–41} The calculations were carried out using the DFT method with a plane wave basis set, implemented in the Vienna Ab initio Simulation Package (VASP).^{42–44} The electron–ion interactions were described by ultrasoft pseudopotentials.⁴⁵ Scalar relativistic electron wave functions for an atomic reference configuration of 5d⁹6s were used to construct the Pt pseudopotential. The Projector augmented wave (PAW) method⁴⁶ is also used to test the accuracy of the ultrasoft pseudopotential calculations. The exchange and correlation energies were calculated using the Perdew–Wang 91 form of the generalized gradient approximation (GGA).⁴⁷ Spin polarization was included in the calculations to account for the magnetic properties of Pt clusters. Finally, spin–orbit coupling was also included in some calculations to assess its effect on the calculated relative stability of Pt clusters.

Below we summarize the parameters that were used in the simulations. A cutoff energy of 300 eV was used for the plane wave basis, which was demonstrated to be sufficient by the convergence test. One k point was used in the finite-cluster calculations. For the infinite clusters, such as a cluster of infinite number of atoms aligned linearly, one k point was used in the nonperiodic directions and eight k points were used in the periodic directions. To eliminate interactions between neighboring clusters, we set the nearest distance between images to no

less than 1.0 nm in the calculations of finite clusters and in the nonperiodic directions for infinite cluster calculations. Initial geometry of a cluster was set with bond distances of 0.27 nm. To test the sensitivity of the initial input of bond length to the result, we used two different initial bond distances for the Pt dimer. The same equilibrium geometry and total energy were obtained. Normal-mode analysis was performed to ensure that the structures we obtained are minima. To explore the Jahn–Teller effect on the stability of various structures, we also distorted the perfect symmetry of initial geometry of a cluster. All the parameters used in the simulations were tested to ensure the calculated binding energy is converged to within 0.01 eV/atom.

The binding energy per atom (E_B) is calculated using

$$E_B = E_{\text{atom}} - E_{\text{cluster}}/N \quad (1)$$

where E_{atom} and E_{cluster} represent the total energy of a single platinum atom and of the cluster of N platinum atoms, respectively. We note that the binding energy as defined in eq 1 is also denoted as the atomization energy per atom.

We defined a bonding energy per bond (E_{bond}) to explore the strength of bonds in a cluster as

$$E_{\text{bond}} = (NE_{\text{atom}} - E_{\text{cluster}})/N_{\text{bond}} \quad (2)$$

where N_{bond} represents the total number of bonds in the cluster. For infinite structures, such as the one shown in Table 1, each of the edge bonds is counted as a half bond. As such, the infinite one-atom Pt nanowire (L _{∞}) in Table 1 has two bonds. The unit of E_{bond} is electronvolts (eV) per bond. We note that the bonding energy defined in eq 2 is an average bonding energy per bond.

The HOMO–LUMO band gap (E_G) is the difference between the energy of the highest occupied level and that of the lowest unoccupied level. The unit of E_G is eV. The magnetic moment per atom (μ) is calculated by















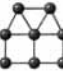
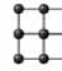
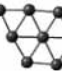

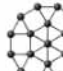


$$\mu = (m_u - m_d)/N \quad (3)$$

where m_u and m_d are the number of electrons of different spin states, with $m_u > m_d$. The unit of μ is Bohr magneton (μ_B) per atom.

3. Results and Discussion

The calculated structures and properties of Pt clusters are given in Tables 1–3. Following our presentations for the Pd³⁹

TABLE 2: Binding Energies (E_B), Bonding Energies (E_{bond}), HOMO–LUMO Band Gaps (E_G), Magnetic Moments (μ), and Bond Distances of Planar Pt Clusters^a

Notation	P ₃	P ₄₋₁ *	P ₄₋₂	P ₅₋₁	P ₅₋₂	P ₅₋₃	P ₆₋₁
Structure							
Symmetry	C _{2v}	D _{4h}	C _{2h}	D _{2h}	C _{2v}	C _{2v}	C _{2v}
Bond distance (Å)	2.47-2.48	2.48	2.51-2.58	2.48	2.45-2.68	2.43-2.51	2.49-2.61
E _B (eV/atom)	2.33	2.61	2.62	2.83	2.84	2.89	3.08
E _{bond} (eV/bond)	2.33	2.61	2.10	2.36	2.03	2.41	2.05
E _G (eV)	0.034	0.12	0.096	0.50	0.12	0.37	1.27
μ (μ _B /atom)	0.0	0.50	0.50	0.40	0.80	0.40	1.00
Notation	P ₆₋₂	P ₆₋₃	P ₆₋₄	P ₇₋₁	P ₇₋₂	P ₈₋₁	P ₈₋₂
Structure							
Symmetry	C _s	C _{2v}	D _{2h}	D _{2h}	C _{2v}	D _{2h}	D _{2h}
Bond distance (Å)	2.47-2.64	2.40-2.48	2.41-2.79	2.55-2.60	2.41-2.59	2.41-2.48	2.47-2.67
E _B (eV/atom)	2.99	3.08	3.23	3.08	3.10	3.21	3.27
E _{bond} (eV/bond)	1.99	2.64	2.42	1.80	2.41	2.57	2.01
E _G (eV)	0.19	0.092	0.54	0.91	0.47	0.10	0.38
μ (μ _B /atom)	0.33	0.33	0.67	0.86	0.86	0.25	0.50
Notation	P ₈₋₃	P ₉₋₁	P ₉₋₂	P ₉₋₃	P ₁₉	P _s	P _d
Structure							
Symmetry	C _{2v}	D _{4h}	C _s	C _{2v}	D _{6h}	D _{4h}	D _{2h}
Bond distance (Å)	2.45-2.70	2.44-2.46	2.48-2.68	2.44-2.60	2.50-2.58	2.54	2.60-2.61
E _B (eV/atom)	3.28	3.41	3.39	3.34	3.68	4.12	4.57
E _{bond} (eV/bond)	2.19	2.56	1.91	2.15	1.94	2.06	1.52
E _G (eV)	0.55	0.39	0.043	0.056	0.083	0.50	0.00
μ (μ _B /atom)	0.50	0.44	0.22	0.44	0.53	0.28	0.00

^a The data for P₄₋₁ (*) were taken from ref 51.

and Ru clusters,⁴¹ the Pt clusters are discussed below according to the dimensionality to which the cluster belongs. For the clarity of our presentation, we use L_N, P_{N-i}, and T_{N-i} to represent one-, two-, and three-dimensional Pd clusters, respectively, where the subscript *N* is the number of atoms in the cluster (also denoted as cluster size) and the subscript *i* is the *i*th structure among the structures studied here at a given size and dimensionality. Further, we omit *i* in the notation if only one structure is studied at a given size and dimensionality. Thus, the notation P₄₋₂ represents that this cluster is the second among all the two-dimensional four-atom structures studied here.

In what follows, we present the effect of spin–orbit coupling on the binding energy of the Pt cluster and then discuss the linear, planar, and three-dimensional Pt clusters.

A. Effect of Spin–Orbit Coupling. To explore the effect of spin–orbit coupling on the binding energy of Pt clusters, we studied Pt clusters consisting of two to six atoms. The cluster of a particular size was chosen as the most stable isomer among the structures shown in Tables 1–3. The results obtained with

and without including spin–orbit coupling in the DFT calculations are plotted in Figure 1 as dashed and solid lines, respectively.

Figure 1 shows clearly that, regardless of the size and structure of the Pt clusters, the binding energy increases by about 0.45 ± 0.04 eV/atom when spin–orbit coupling is included in the calculation. The results show that spin–orbit coupling does not affect the relative stability of various isomers, though the binding energy of Pt clusters increases by the inclusion of spin–orbit coupling. In addition, the results obtained from using the pseudopotential and PAW methods are essentially the same, as also shown in Figure 1, which agrees with results from studies on the Rh clusters.⁴⁰

B. Linear Pt Chains. For the linear Pt configuration, many researchers focused on the dimer and trimer. To the best of our knowledge, little is known about the Pt chains with more than three atoms. This is due to the fact that the linear structures are not considered as stable structures. However, a molecular dynamics simulation shows that the tendency for chain formation

TABLE 3: Binding Energies (E_B), Bonding Energies (E_{bond}), HOMO–LUMO Band Gaps (E_G), Magnetic Moments (μ), and Bond Distances of Three-Dimensional Pt Clusters





























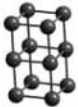
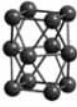


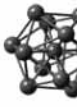



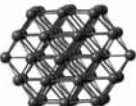
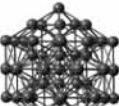

Notation	T_4^*	T_{5-1}	T_{5-2}	T_{6-1}	T_{6-2}	T_{7-1}	T_{7-2}
Structure							
Symmetry	C_s	D_{3h}	C_{4v}	O_h	C_{2v}	C_{2v}	C_1
Bond distance (Å)	2.56-2.67	2.57-2.63	2.56-2.63	2.61	2.51-2.57	2.53-2.79	2.60-2.73
E_B (eV/atom)	2.68	2.91	2.89	3.07	3.08	3.18	3.21
E_{bond} (eV/bond)	1.79	1.62	1.81	1.54	2.05	1.59	1.50
E_G (eV)	0.28	0.63	0.22	0.02	2.03	0.25	1.25
μ (μ_B /atom)	0.50	0.80	0.40	1.00	1.33	0.29	1.14
Notation	T_{7-3}	T_{7-4}	T_{7-5}	T_{8-1}	T_{8-2}^*	T_{8-3}	T_{9-1}
Structure							
Symmetry	C_{3v}	C_s	C_1	C_s	O_h	C_1	C_s
Bond distance (Å)	2.52-2.60	2.61-2.69	2.56-2.84	2.52-2.72	2.54	2.55-2.68	2.54-2.73
E_B (eV/atom)	3.22	3.18	3.19	3.31	3.34	3.32	3.43
E_{bond} (eV/bond)	1.88	1.48	1.49	1.89	2.23	1.66	1.47
E_G (eV)	0.067	0.49	0.16	0.12	1.13	0.29	0.44
μ (μ_B /atom)	0.29	0.85	0.57	0.75	1.00	0.75	0.89
Notation	T_{9-2}^*	T_{9-3}	T_{9-4}	T_{9-5}	T_{10-1}	T_{10-2}	T_{10-3}
Structure							
Symmetry	C_{4v}	C_s	C_1	C_1	S_2	D_{4h}	C_1
Bond distance (Å)	2.51-2.69	2.60-2.90	2.50-3.02	2.54-2.91	2.56-2.74	2.53-2.69	2.56-2.96
E_B (eV/atom)	3.47	3.42	3.33	3.41	3.51	3.50	3.46
E_{bond} (eV/bond)	1.95	1.46	1.50	1.53	1.59	1.75	1.44
E_G (eV)	0.27	1.06	0.17	0.099	0.17	0.52	0.25
μ (μ_B /atom)	0.67	0.89	0.44	0.67	0.40	0.80	0.80
Notation	T_{10-4}	T_{10-5}	T_{10-6}	T_{11-1}	T_{11-2}	T_{11-3}	T_{11-4}
Structure							
Symmetry	C_1	C_1	C_1	C_s	C_1	C_1	C_s
Bond distance (Å)	2.51-2.81	2.49-2.72	2.57-2.72	2.52-2.82	2.60-2.95	2.48-2.76	2.44-2.73
E_B (eV/atom)	3.64	3.57	3.49	3.55	3.61	3.67	3.60
E_{bond} (eV/bond)	1.58	1.78	1.45	1.45	1.37	1.68	1.47
E_G (eV)	0.19	0.13	0.19	0.21	0.19	0.063	0.23
μ (μ_B /atom)	0.60	0.40	0.80	0.73	0.54	0.18	0.55

TABLE 3 (Continued)^a

Notation	T ₁₂₋₁ [*]	T ₁₂₋₂	T ₁₃₋₁	T ₁₃₋₂ [*]	T ₁₃₋₃ [*]	T ₁₃₋₄ [*]	T ₁₉₋₁
Structure							
Symmetry	D _{2h}	D _{2h}	C _s	C _{4v}	C _{2h}	O _h	O _h
Bond distance (Å)	2.50-2.57	2.60-2.72	2.39-2.88	2.50-2.68	2.56-2.74	2.69	2.76
E _B (eV/atom)	3.65	3.65	3.71	3.68	3.58	3.60	4.01
E _{bond} (eV/bond)	2.19	1.56	1.46	1.99	1.11	1.30	1.31
E _G (eV)	0.025	0.15	0.31	0.42	0.11	0.76	0.083
μ (μ _B /atom)	0.50	0.33	0.61	0.62	0.15	0.46	0.53
Notation	T ₁₉₋₂	T ₅₅₋₁	T ₅₅₋₂	T _∞			
Structure							
Symmetry	C _s	C ₁	C ₁				
Bond distance (Å)	2.50-2.70	2.72-2.89	2.73-2.89	2.81			
E _B (eV/atom)	3.98	4.44	4.46	5.45			
E _{bond} (eV/bond)	2.04	1.69	1.51	0.91			
E _G (eV)	0.12	0.14	0.13	0.00			
μ (μ _B /atom)	0.11	0.18	0.22	0.00			

^a The data for T₄, T₈₋₂, T₉₋₂, T₁₂₋₁, T₁₃₋₂, T₁₃₋₃, and T₁₃₋₄ (*) were taken from ref 51.

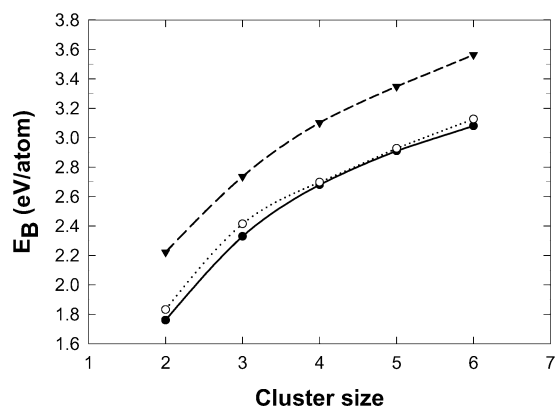


Figure 1. Binding energy (E_B) of Pt clusters as a function of cluster size obtained using the ultrasoft pseudopotential method (●), PAW method (○), and PAW including spin-orbit coupling (▼). For each size, the most stable isomer among Tables 1–3 is chosen.

is strong for Pt.⁴⁸ Furthermore, a recent experiment demonstrated that there exists a long-range ferromagnetic order for one-dimensional nanostructures of Co on a surface.⁴⁹ This inspired us to investigate linear Pd and Pt chains and to explore the electromagnetic properties of these structures. In our previous work we found that the linear Pd chains are indeed ferromagnetic with chain length up to infinite.⁴⁵

The results for linear Pt chains are given in Table 1, which presents the calculated bond distances, binding energies, bonding energies, HOMO–LUMO band gaps, and magnetic moments of eight finite chains and one infinite chain.

As shown in Table 1, the binding energies of the linear Pt chains increase with cluster size except for L₆, which is only as stable as L₅. This unusual behavior is also accompanied by the following phenomenon: namely, the bonds at the edge become shorter than the middle bonds for the linear clusters with chain lengths longer than six atoms. Furthermore, the five-atom Pt chain as shown in Table 1 has the shortest bond lengths among all the linear clusters, which provides maximum overlap among bonding orbitals and may explain the formation of stronger bonds in this cluster.

Figure 2a depicts the HOMO–LUMO band gap and magnetic moment as a function of cluster size for the linear Pt clusters. The band gaps of the clusters change in an oscillatory manner with cluster size. A similar trend holds for the magnetic moments of these clusters. Furthermore, highly magnetic clusters tend to have large band gaps except for L₅. These observations are very similar to those observed for the palladium linear chains.³⁹ However, the infinite and L₅ Pt chains are paramagnetic, while all of the linear Pd clusters studied in ref 39 are ferromagnetic. In addition, the overall magnetism of linear Pt clusters is less pronounced compared to that of the linear Pd clusters.³⁹

In the effort to explore whether a zigzag quasi-linear structure would be preferred energetically than its linear isomer listed in Table 1, we investigated the stability of a zigzag Pt trimer. This was done by arranging three Pt atoms initially in a geometry of 120° among three atoms with two bonds of 2.50 Å and then allowing it to relax. The result shows that this zigzag structure is relaxed to a bond angle of 141.6° with two bonds of 2.33 Å

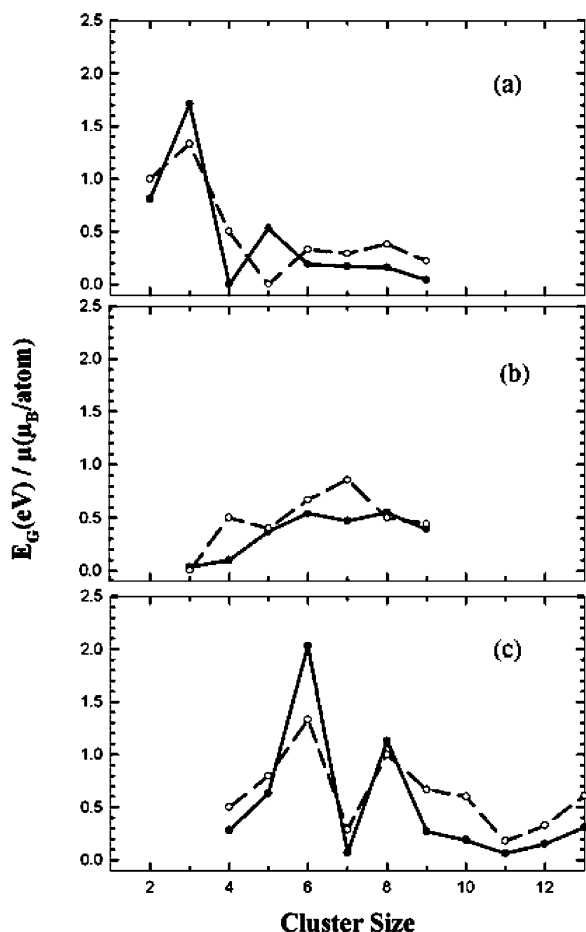


Figure 2. HOMO–LUMO energy gap (E_G , solid line) and magnetic moment (μ , dashed line) as a function of cluster size for linear (a), planar (b), and three-dimensional (c) Pt clusters. In each dimensionality, when more than one structure is available, we plot the most stable one.

and has a binding energy of 2.14 eV/atom, which is less stable than the linear trimer shown in Table 1. In addition, this zigzag Pt trimer possesses a magnetic moment and HOMO–LUMO energy gap of $0.67 \mu_B/\text{atom}$ and 0.11 eV, respectively. These values are smaller than those of the linear trimer shown in Table 1.

Before discussing the other types of Pt clusters, we compare our results with those obtained for the Pt dimer and trimer in the literature. For the Pt dimer, our calculated bond distance is 2.34 Å and the binding energy per atom is 1.76 eV. These values are in excellent agreement with the experimental bond length of 2.34 Å and dissociation energy of 1.83 ± 0.08 eV/atom.¹¹ However, the bond length is shorter than the 2.40–2.45 Å reported using different computational methods.^{6,9,10} Our binding energy agrees less satisfactorily with 1.92 eV from a full multiple scattering, real-space Green's function calculation,²¹ 1.15 eV using the B3PW91 with a Gaussian (3s2p2d) basis set,¹⁰ 1.57 eV from the dispersed fluorescence spectroscopy,²⁹ and 1.65 eV from the non-self-consistent Harris functional version of LDA.⁹ For the Pt trimer, our calculated bond length of 2.35 Å is slightly shorter than the previously reported results of 2.38 Å⁹ and 2.40 Å.¹⁰ The binding energy per atom of 2.18 eV agrees with 2.16 eV⁹ but is larger than 1.45 eV.¹⁰

C. Planar Pt Clusters. Twenty-one planar Pt clusters were investigated in this work, and their results are summarized in Table 2.

The ground-state geometry of the planar Pt cluster P_3 is an isosceles triangle with two bond lengths of 2.47 Å and one of

2.48 Å. Its binding energy is 2.33 eV/atom and the ground state is singlet. Our calculated bond lengths are in good agreement with the value of 2.45 Å obtained from the DFT-GGA calculations,²⁰ but are shorter than the 2.52 Å value from the nonlocal DFT calculations¹⁶ and 2.58 Å.⁹ Our calculated binding energy is slightly less than 2.40 eV/atom.⁹ Wang and Carter⁸ also reported a singlet ground state, but Lin et al.²⁰ reported a triplet ground state.

Our results for the planar Pt tetramer show that the stabilities of square and rhombus structures are essentially the same, although their bond lengths are different. This trend agrees with the results by Yang et al.⁹ In our previous studies of Pd³⁹ and Rh⁴⁰ clusters, the square Pd and Rh clusters were found to be slightly more stable than their corresponding rhombus isomers.

The planar Pt clusters shown in Table 2 can be divided into three classes according to the composition of two basic building blocks, i.e., triangular unit (P_3) and square unit (P_4). The first class consists of structures of triangular units only, such as P_3 , P_{4-2} , and P_{5-1} . The second is the structures consisting of square units only, such as P_{4-1} , P_{6-3} , and P_{8-1} . The third class is the structures with a mixture of triangular and square units. Examples of this class include P_{5-3} and P_{6-4} . In Figure 3a we plot the binding energies of these planar Pt clusters as a function of size according to this classification. It shows that the stabilities of isomers that belong to different classes are very similar. However, the bonding energies of these planar Pt isomers, shown in Figure 3b, illustrate that the bonding energies of square-unit-only clusters (the second class), are substantially higher than those of triangular-unit-only isomers (the first class). On the other hand, less coordination numbers per atom are in the square-unit-only clusters. Since the stability of a cluster is determined by two factors, namely coordination numbers and bonding energy, the similar stability among the three classes of planar clusters shown in Figure 3a is thus the consequence of the balance between these two factors.

Furthermore, we found that the triangular-unit-only clusters P_{4-2} and P_{9-2} are nearly as stable as their corresponding square-only isomers P_{4-1} and P_{9-1} , respectively. However, the infinite triangular-unit-only structure, P_d , becomes substantially more stable than the infinite square-only structure, P_s . The binding energy of the most stable isomer is plotted as a function of cluster size in Figure 4. The binding energy of planar Pt clusters (see the open circles) increases with cluster size except for the six-atom cluster, which is more stable than the seven-atom cluster. This may be due to an optimal combination of triangular and square units in the six-atom Pt cluster.

The comparison of the relative stability of planar and linear clusters shown by the open circles (○) and filled circles (●), respectively, in Figure 3 demonstrated clearly that the planar clusters are much more stable than their linear isomers. This can be understood by the fact that the coordination numbers per atom in planar structures increase substantially. Furthermore, the difference in binding energy between the linear and the planar isomers increases more dramatically with the increase of cluster size.

The electronic and magnetic properties of the planar Pt clusters are depicted in Figure 2b. Similar to the linear ones, the planar clusters of higher HOMO–LUMO band gaps possess higher magnetic moments in most cases.

D. Three-Dimensional Pt Clusters. Results obtained for 38 three-dimensional Pt clusters are given in Table 3, where their structures, bond distances, binding energies, bonding energies, HOMO–LUMO band gaps, and magnetic moments are provided.

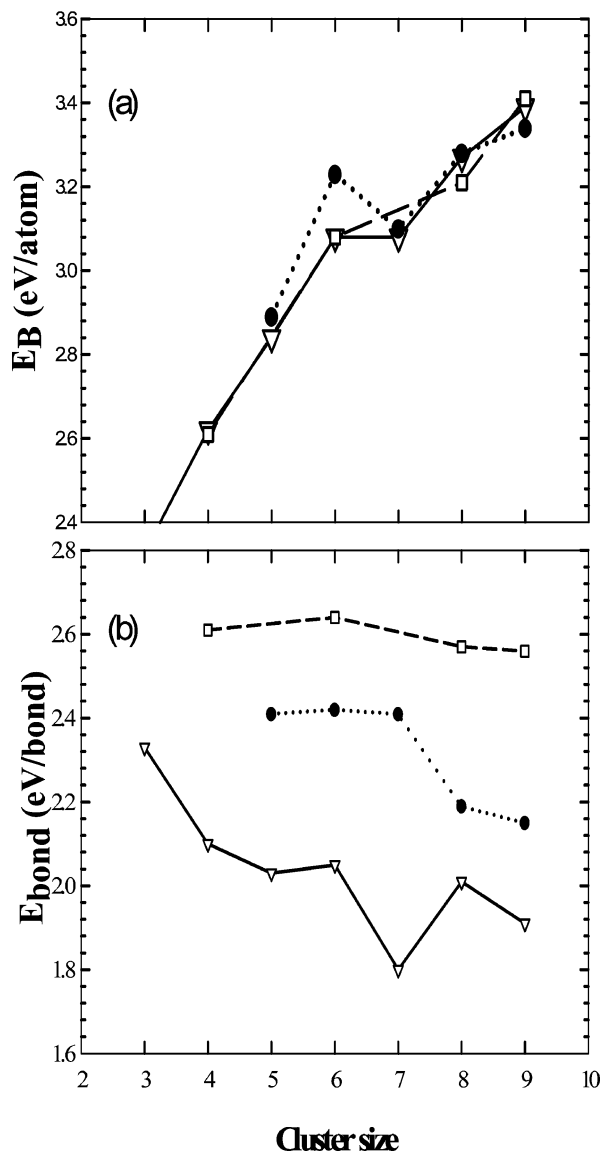


Figure 3. Binding energies (E_B) (a) and bonding energies (E_{bond}) (b) as a function of cluster size for planar Pt clusters. The symbols ∇ , \square , and \bullet represent clusters composed of triangular, square, and triangular-square units, respectively.

We first discuss the binding strength of these three-dimensional Pt clusters and the relative stability among them and over other lower dimensional structures, in particular planar structures. As we expected, the binding energy of these three-dimensional clusters increases with cluster size, which is clearly illustrated by the triangular symbols in Figure 4. The same observation was made from our studies on Pd³⁹ and Rh⁴⁰ clusters. More interestingly, Figure 4 shows similar binding energies between the planar and three-dimensional isomers up to at least nine-atom clusters. It also shows that the planar structure P_{6-4} of the six-atom Pt clusters was more stable than its three-dimensional isomers.

We should point out that a similar conclusion was also drawn by Yang and co-workers in ref 9. However, their conclusion was based on the comparison between the binding energies of P_{6-2} and T_{6-1} , which is opposite our results shown in Tables 2 and 3.

The fact that small planar Pt clusters are as stable as their three-dimensional isomers suggests that a lot of stable isomers may be found since many different but possible ways of bonding Pt atoms exist. One immediate prediction is the existence of

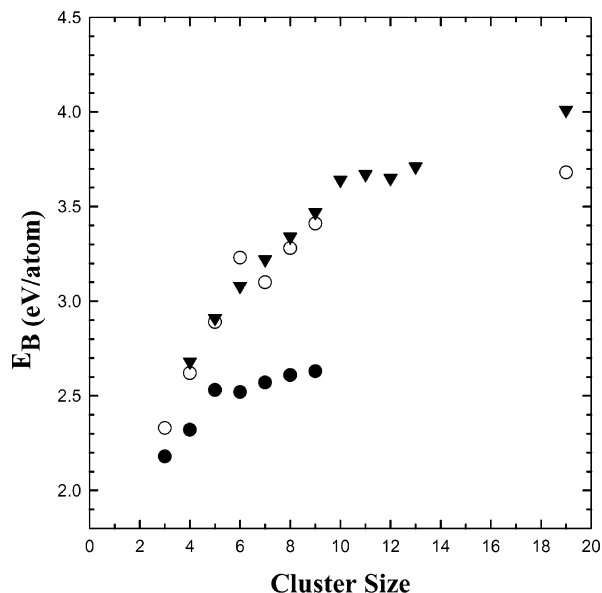


Figure 4. Binding energy (E_B) as a function of cluster size for linear (\bullet), planar (\circ), and three-dimensional (\blacktriangledown) Pt clusters. In each dimensionality, when more than one structure is available, we plot the most stable one.

stable layered structures. Therefore, two sets of clusters were designed and investigated. They are the 13-atom and 19-atom clusters, and the results are given in Table 3. The layered structures T_{13-1} and T_{13-2} are indeed more stable than their spherical close-packed isomers T_{13-3} and T_{13-4} . For the 19-atom clusters, the bilayer structure T_{19-2} is as stable as the spherical close-packed structure T_{19-1} . These results are different from our observations on the Pd clusters, where spherical clusters, such as the 13-atom icosahedral Pd cluster, are more stable than other three-dimensional ones.³⁹ It is also worthwhile to point out that the tetrahedral structure of the 10-atom Pt cluster shows substantial stability over its other isomers.

Among many highly symmetric structures, the relaxed Pt clusters are mostly distorted from their perfect symmetry due to the Jahn–Teller effect. For instance, the tetrahedral structure of T_4 with T_d symmetry is distorted to C_s symmetry. This has been shown by Lin et al. from their DFT calculations, even though their calculated T_4 structure had a D_{2d} symmetry.²⁰ This symmetry reduction also occurs for clusters such as 13-atom and 55-atom Pt clusters.

The HOMO–LUMO band gap and magnetic moment of three-dimensional Pt clusters as cluster size are plotted in Figure 2c. Very similar to the linear and planar clusters, a highly magnetic three-dimensional Pt cluster tends to have a high HOMO–LUMO band gap.

To further correlate the structure and electronic properties, we plot the spin-resolved total density of states (DOS) for seven clusters in Figure 5. As we expected, the DOS increases with cluster size as shown clearly from top to bottom in Figure 5. To assist our discussion, we divide six of the seven clusters in Figure 5 into two groups. The first group consists of T_{6-1} , T_{8-3} , and T_{12-2} , which has maximum triangular units. The second group includes T_{6-2} , T_{8-2} , and T_{12-1} , which has maximum square units. One interesting feature is that the clusters of the first group have the lowest energy states compared to their isomers in the second group. For instance, the lowest energy state for T_{6-1} occurs below -6 eV, while that for T_{6-2} occurs above -6 eV. This normally indicates that the first group clusters are more stable than the second group members. However, the significant contribution from the other widely

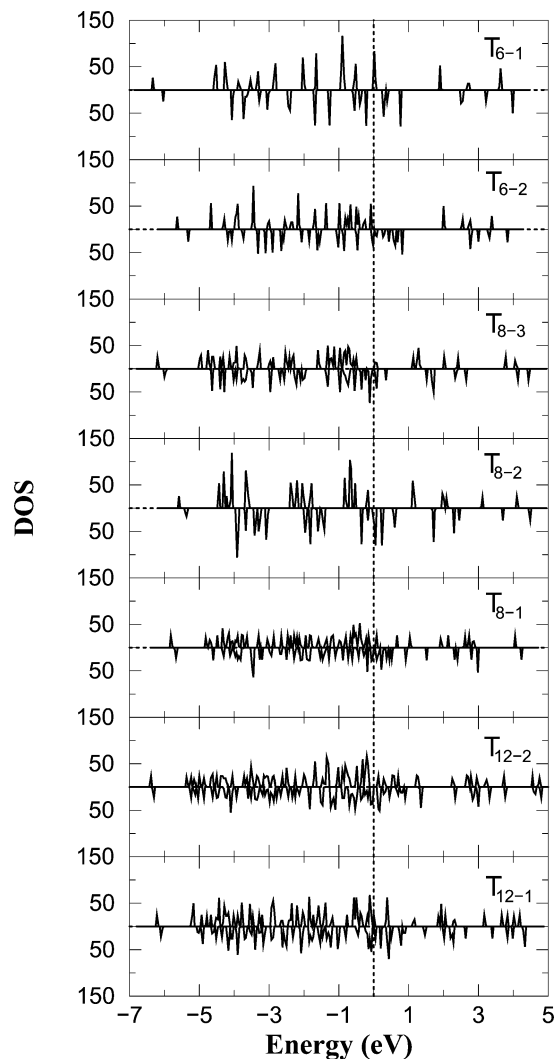


Figure 5. Spin-resolved total density of states (DOS) of seven Pt clusters. The vertical dashed line is the Fermi level. The intensity of the DOS is in an arbitrary unit.

distributed states to the cluster stability as shown in Figure 5 also determines the cluster stability. As such, these two groups of clusters have similar binding energies.

We also investigated the charge distribution of these two groups of clusters. All the atoms in the six-atom and eight-atom clusters in Figure 5 are neutral. In contrast, atoms in the middle layers of the 12-atom clusters are slightly negatively charged while the atoms in the other two layers are positively charged. Furthermore, the difference in the charge distribution among atoms occurs only in the p characterized charges. Therefore, we focus our discussion on the distribution of these p characterized charges. There are two types of atoms in T_{12-1} , namely the atoms in the middle layer and the others, and three types of atoms in T_{12-2} , namely the atoms in the middle layer and the other two types in the top and bottom layers as shown in Figure 6. Figure 6 also shows the distribution of the p charges on these atoms. For both clusters, the charge distribution in the middle layer atoms is substantially higher than those of the other layer atoms. The same charge distribution of the s and d characters but different distribution of the p character for all the atoms in the T_{12-1} and T_{12-2} clusters indicates that the s and d orbitals are hybridized while the p orbitals remain in their atomic form in these clusters.

We discuss now the possible changes in DOS if a cluster is distorted by a comparison between the T_{8-1} and T_{8-2} clusters

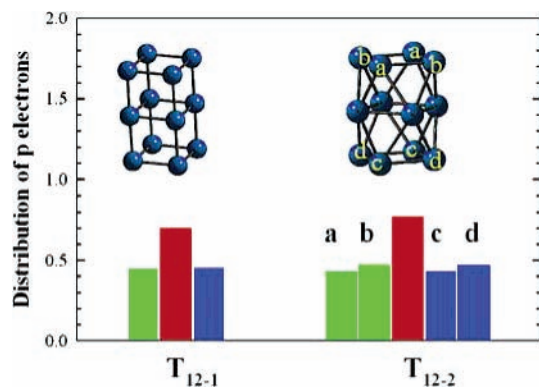


Figure 6. Distribution of $5d_{5/2}$ electrons for T_{12-1} (left) and T_{12-2} (right) clusters. The distribution of $5d_{5/2}$ electrons for the atoms in the top, middle, and bottom layers are represented by green, red, and blue bars, respectively. The four atoms in each layer in the T_{12-1} cluster have identical distribution. In the T_{12-2} cluster there are two types of atoms in the top layer labeled as a and b and in the bottom layer labeled as c and d. The a–a and c–c distances are longer than the b–b and d–d distances, respectively. The four atoms in the middle layer of the T_{12-2} cluster are identical.

in Table 3. The T_{8-1} cluster can be considered as a distortion of the T_{8-2} cluster by pushing the two diagonal atoms in the same layer toward each other. Our calculation shows that the distorted T_{8-1} cluster is only slightly less stable than its original structure, T_{8-2} . However, such a distortion changes the semiconductor T_{8-2} into a conductor T_{8-1} . Furthermore, their DOS values in Figure 5 show clearly that the DOS has changed dramatically if a distortion occurs. These energetically possible Pt isomers with different HOMO–LUMO band gaps and DOS could be very promising candidates as fluorophores in photoelectron transfer sensors, because substantial change in the HOMO–LUMO band gap of a system under certain structural distortion is one of the critical quantities for fluorophores.⁵⁰

Following our previous work on the Pd clusters,³⁹ we correlate here the binding energy, HOMO–LUMO band gap, and magnetic moments of Pt clusters with their size and structures. The structure factor, S_f , is used to quantify the Pt structures shown in Tables 1–3 and is calculated by

$$S_f = g_s g_d \bar{N}_c \quad (4)$$

where \bar{N}_c is the coordination number per atom of the cluster and g_s and g_d are the factors to account for symmetry and the dimensionality of the structure, respectively. For the linear, planar, and three-dimensional structures, we set $g_d = 0.8, 0.9,$ and $1,$ respectively. The introduction of g_d is to distinguish isomers of the same averaged coordination number but with different dimensionality. In cases that one cannot distinguish two isomers after taking the averaged coordination number and dimensionality into account, the introduction of another symmetry factor, g_s , is needed. In most of the structures encountered here, we set $g_s = 1$ except for $P_{5-1}, P_{6-1}, T_{7-5}, T_{9-1}, T_{10-2}, T_{10-6},$ and $T_{11-4},$ where we set $g_s = 1.05,$ and T_{7-2} where we set $g_s = 1.1.$

In Figure 7, the binding energy, HOMO–LUMO band gap, and magnetic moments of Pt clusters of less than 13 atoms are plotted as a function of cluster size and structure factor. The top contour is the binding energy as a function of cluster size and structure factor. This plot shows clearly that many isomers are energetically possible, which leads us to conclude a fluxional characteristic in the structures of Pt clusters. The middle contour shows how the HOMO–LUMO band gap changes with cluster size and structure. It illustrates that most of the Pt clusters

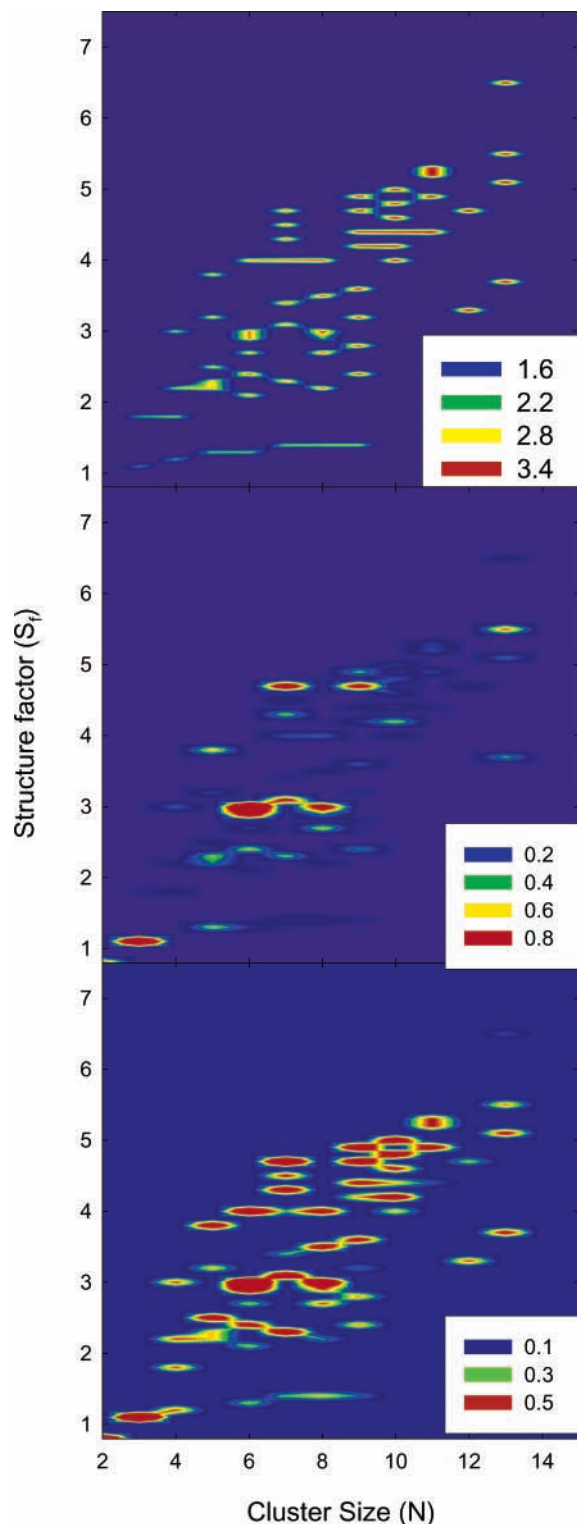


Figure 7. Contour plots of the binding energy (top), HOMO–LUMO band gap (middle), and magnetic moment (bottom) of Pt clusters as a function of cluster size (N) and structure factor (S_i).

studied here are good conductors. The bottom plot in Figure 7 depicts the magnetic moments of Pt clusters as a function of cluster size and structure. Most of the Pt clusters are ferromagnetic. More interesting is the comparison between Figure 7 and that for Pd clusters.³⁹ Two major differences can be found between the clusters formed by these two elements. First, the stability of Pt clusters is less dimensionally dependent. This is reflected by the wide spread of the same intensity in the top contour in Figure 7 compared to a rather narrow distribution of

the intensity for Pd clusters. Second, the Pt clusters of higher dimensionality tend to have higher magnetic moments. In contrast, the linear Pd clusters tend to have high magnetic moments. Therefore, Figure 7 could be used as fingerprint to identify clusters formed from different elements.

4. Conclusions

Structural, energetic, electronic, and magnetic properties of 70 platinum clusters were calculated using DFT with a plane wave basis set. The effect of spin–orbit coupling on the binding energy of the cluster was investigated. The results show that the relative stability of Pt clusters is not affected with the inclusion of spin–orbit coupling, but the binding energy of the cluster increases when spin–orbit coupling is considered in the calculations.

The binding energies of planar and three-dimensional isomers are very close to each other at least within nine-atom Pt clusters. This is different from the Pd clusters, where the planar Pd clusters are less stable than the three-dimensional ones. Due to the similar stability between planar and three-dimensional Pt clusters, many isomers are energetically possible. Some layered structures are at least as stable as the spherical isomers. Moreover, the six-atom Pt cluster has very surprising properties. Its linear structure represents a characteristic change in the bond distances. This means that the bond lengths of the edge atoms are the shortest after the linear cluster size becomes larger than six. Furthermore, the six-atom planar structure is more stable than its three-dimensional isomers. We also found that the 10-atom tetrahedral Pt cluster is substantially more stable than its other isomers investigated in this work. Our calculations showed that there exist more stable structures than the icosahedron and cubooctahedron for 13-atom Pt clusters.

Both the HOMO–LUMO band gap and magnetic moment change in an oscillatory manner with cluster size. Strong correlation is also observed: Highly magnetic clusters tend to have large HOMO–LUMO band gaps. The DOS and detailed analysis of the charge distribution show that the middle layer atoms are slightly negative charged in the T_{12-1} and T_{12-2} clusters.

Using the structure factor to quantify each Pt cluster structure studied in this work, we are able to correlate the binding energy, HOMO–LUMO band gap, and magnetic moment of the Pt clusters with their size as well as structure. Comparison between the contour plots of Pt and Pd clusters indicates that this contour plot (Figure 7) could be used as a fingerprint for identifying clusters formed by different elements.

Acknowledgment. We acknowledge the start-up fund from Southern Illinois University at Carbondale (SIUC) and the Materials Technology Center at SIUC for support. We are also greatly indebted to Prof. Qingfeng Ge for discussion and comments.

Supporting Information Available: Tables containing the energies of linear Pt chains, planar Pt clusters, and three-dimensional Pt clusters. This material is available free of charge via the Internet at <http://pubs.acs.org>.

References and Notes

- (1) *Clusters of atoms and molecules*; Haberland, H., Ed.; Springer-Verlag: New York, 1994.
- (2) Sun, S.; Murray, C. B.; Weller, D.; Folks, L.; Moser, A. *Science* **2000**, *287*, 1989.

- (3) (a) Smith, G. V.; Tjandra, S.; Musoiu, M.; Wiltowski, T.; Notheisz, F.; Bartok, M.; Hannus, I.; Ostgard, D.; Malhotra, V. *J. Catal.* **1996**, *161*, 441. (b) Wei, J. M.; Iglesia, E. *J. Phys. Chem. B* **2004**, *108*, 4094.
- (4) Majetich, S. A.; Jin, Y. *Science* **1999**, *284*, 470.
- (5) Gambardella, P.; Rusponi, S.; Veronese, M.; et al. *Science* **2003**, *300*, 1130.
- (6) Balasubramanian, K. *J. Chem. Phys.* **1987**, *87*, 6573.
- (7) Xu, W.; Schierbaum, K. D.; Goepel, W. *Int. J. Quantum Chem.* **1997**, *62*, 427.
- (8) Wang, H.; Carter, E. A. *J. Phys. Chem.* **1992**, *96*, 1197.
- (9) Yang, S. H.; Drabold, D. A.; Adams, J. B.; Ordejón, P.; Glassford, K. *J. Phys.: Condens. Matter* **1997**, *9*, L39.
- (10) Li, T.; Balbuena, P. B. *J. Phys. Chem. B* **2001**, *105*, 9943.
- (11) Gupta, S. K.; Nappi, B. M.; Gingerich, K. A. *Inorg. Chem.* **1981**, *20*, 966.
- (12) Bigot, B.; Minot, C. *J. Am. Chem. Soc.* **1984**, *106*, 6601.
- (13) Cheng, H.-P.; Ellis, D. E. *J. Chem. Phys.* **1991**, *94*, 1.
- (14) García-Rodeja, J.; Rey, C.; Gallego, L. J.; Alonso, J. A. *Phys. Rev. B* **1994**, *49*, 8495.
- (15) Dai, D.; Balasubramanian, K. *J. Chem. Phys.* **1995**, *103*, 8.
- (16) Kua, J.; Goddard, W. A., III. *J. Phys. Chem. B* **1998**, *102*, 9481.
- (17) (a) Cui, Q.; Musaev, D. G.; Morokuma, K. *J. Phys. Chem. A* **1998**, *102*, 6373. (b) Cui, Q.; Musaev, D. G.; Morokuma, K. *J. Chem. Phys.* **1998**, *108*, 8418.
- (18) (a) Majumdar, D.; Dai, D.; Balasubramanian, K. *J. Chem. Phys.* **2000**, *113*, 7919. (b) Majumdar, D.; Dai, D.; Balasubramanian, K. *J. Chem. Phys.* **2000**, *113*, 7928.
- (19) Gronbeck, H.; Andreoni, W. *Chem. Phys.* **2000**, *262*, 1.
- (20) Lin, X.; Ramer, N. J.; Rappe, A. M.; Hass, K. C.; Schneider, W. F.; Trout, B. L. *J. Phys. Chem. B* **2001**, *105*, 7739.
- (21) Ankudinov, A. L.; Rehr, J. J.; Low, J. J.; Bare, S. R. *J. Chem. Phys.* **2002**, *116*, 1911.
- (22) Pavlyukh, Y.; Hübner, W. *Eur. Phys. J. D* **2002**, *21*, 239.
- (23) Hui, L.; Pederiva, F.; Guanghou, W.; Baolin, W. *Chem. Phys. Lett.* **2003**, *381*, 94.
- (24) Spisak, D.; Hafner, J. *Phys. Rev. B* **2003**, *67*, 214416.
- (25) Tian, W. Q.; Ge, M.; Sahu, B. R.; Wang, D.; Yamada, T.; Mashiko, S. *J. Phys. Chem. A* **2004**, *108*, 3806.
- (26) Lombardi, J. R.; Davis, B. *Chem. Rev.* **2002**, *102*, 2431.
- (27) Airola, M. B.; Morse, M. D. *J. Chem. Phys.* **2002**, *116*, 1313.
- (28) Taylor, S.; Lemire, G. W.; Hamrick, Y. M.; Fu, Z.; Morse, M. D. *J. Chem. Phys.* **1988**, *89*, 5517.
- (29) Fabbri, J. C.; Langenberg, J. D.; Costello, Q. D.; Morse, M. D.; Karlsson, L. *J. Chem. Phys.* **2001**, *115*, 7543.
- (30) Pyykko, P. *Chem. Rev.* **1988**, *88*, 563.
- (31) Yang, L.; DePristo, A. E. *J. Chem. Phys.* **1994**, *100*, 725.
- (32) Sachdev, A.; Masel, R. I.; Adams, J. B. *Z. Phys. D* **1993**, *26*, 310.
- (33) Uppenbrink, J.; Wales, D. J. *Z. Phys. D* **1993**, *26*, 258.
- (34) Watari, N.; Ohnishi, S. *J. Chem. Phys.* **1997**, *106*, 7531.
- (35) Watari, N.; Ohnishi, S. *Phys. Rev. B* **1998**, *58*, 1665.
- (36) (a) Aprà, E.; Fortunelli, A. *J. Mol. Struct. (THEOCHEM)* **2000**, *501–502*, 251. (b) Aprà, E.; Fortunelli, A. *J. Phys. Chem. A* **2003**, *107*, 2934.
- (37) Massen, C.; Mortimer-Jones, T. V.; Johnston, R. L. *J. Chem. Soc., Dalton Trans.* **2002**, 4375.
- (38) Varga, S.; Fricke, B.; Nakamatsu, H.; Mukoyama, T.; Anton, J.; Geschke, D.; Heitmann, A.; Engel, E.; Bastug, T. *J. Chem. Phys.* **2000**, *112*, 3499.
- (39) Zhang, W.; Ge, Q.; Wang, L. *J. Chem. Phys.* **2003**, *118*, 5793.
- (40) Wang, L.; Ge, Q. *Chem. Phys. Lett.* **2002**, *366*, 368.
- (41) Zhang, W.; Zhao, H.; Wang, L. *J. Phys. Chem. B* **2004**, *108*, 2140.
- (42) Kresse, G.; Hafner, J. *Phys. Rev. B* **1993**, *47*, 558.
- (43) Kresse, G.; Furthmüller, J. *Phys. Rev. B* **1996**, *54*, 11169.
- (44) Kresse, G.; Furthmüller, J. *Comput. Mater. Sci.* **1996**, *6*, 15.
- (45) Vanderbilt, D. *Phys. Rev. B* **1990**, *47*, 7892.
- (46) Kresse, G.; Joubert, J. *Phys. Rev. B* **1999**, *59*, 1758.
- (47) Perdew, J. P.; Chevary, J. A.; Vosko, S. H.; Jackson, K. A.; Pederson, M. R.; Singh, D. J.; Fiolhais, C. *Phys. Rev. B* **1992**, *46*, 6671.
- (48) Mayer, M.; Kruger, S.; Rosch, N. *J. Chem. Phys.* **2001**, *115*, 4411.
- (49) Bahn, S. R.; Jacobsen, K. W. *Phys. Rev. Lett.* **2001**, *87*, 266101.
- (50) Gambardella, P.; Dallmeyer, A.; Maiti, K.; Malagoli, M. C.; Eberhardt, W.; Kern, K.; Carbone, C. *Nature* **2002**, *416*, 301.
- (51) de Silva, A. P.; Gunaratne, H. Q. N.; Gunnlaugsson, T.; Huxley, A. J. M.; McCoy, C. P.; Rademacher, J. T.; Rice, T. E. *Chem. Rev.* **1997**, *97*, 1515.
- (52) Zhang, W.; Xiao, L.; Hirata, Y.; Pawluk, T.; Wang, L. *Chem. Phys. Lett.* **2004**, *383*, 67.